Neuropathological and biochemical investigation of Hereditary Ferritinopathy cases with ferritin light chain mutation: Prominent protein aggregation in the absence of major mitochondrial or oxidative stress

M. Kurzawa-Akanbi*† (iD), M. Keogh*‡§, E. Tsefou†, L. Ramsay¶**, M. Johnson¶, S. Keers¶, L. WSA Ochieng†, A. McNair†, P. Singh†, A. Khan‡, A. Pyle*, G. Hudson*, P. G. Ince**, J. Attems††, J. Burn*‡‡, P. F. Chinnery*§ and C. M. Morris†¶

*Biosciences Institute,Newcastle University,International Centre for Life, Newcastle upon Tyne, UK, †Wolfson Building, Newcastle University, Newcastle upon Tyne, UK, ‡Department of Neurology, Royal Victoria Infirmary, Newcastle upon Tyne, UK, §MRC Mitochondrial Biology Unit, Department of Clinical Neurosciences, Cambridge Biomedical Campus,Cambridge University, Cambridge, UK, ¶Newcastle Brain Tissue Resource,Translational and Clinical Research Institute,Newcastle University, Newcastle upon Tyne, UK, **Academic Unit of Pathology, Royal Hallamshire Hospital, Sheffield, UK, ††Cellular Pathology, Royal Victoria Infirmary,Newcastle upon Tyne Hospitals NHS Foundation Trust, Newcastle upon Tyne, UK and ‡‡Northern Genetics Service, Newcastle upon Tyne Hospitals NHS Foundation Trust,International Centre for Life, Newcastle upon Tyne, UK*

M. Kurzawa-Akanbi, M. Keogh, E. Tsefou, L. Ramsay, M. Johnson, S. Keers, L. WSA Ochieng, A. McNair, P. Singh, A. Khan, A. Pyle, G. Hudson, P. G. Ince, J. Attems, J. Burn, P. F. Chinnery and C. M. Morris (2020) *Neuropathology and Applied Neurobiology*
Neuropathological and biochemical investigation of Hereditary Ferritinopathy cases with ferritin light chain mutation: Prominent protein aggregation in the absence of major mitochondrial or oxidative stress

Aims: Neuroferritinopathy (NF) or hereditary ferritinopathy (HF) is an autosomal dominant movement disorder due to mutation in the light chain of the iron storage protein ferritin (FTL). HF is the only late-onset neurodegeneration with brain iron accumulation disorder and study of HF offers a unique opportunity to understand the role of iron in more common neurodegenerative syndromes. **Methods**: We carried out pathological and biochemical studies of six individuals with the same pathogenic *FTL* mutation. **Results**: CNS pathological changes were most prominent in the basal ganglia and cerebellar dentate, echoing the normal pattern of brain iron accumulation. Accumulation of ferritin and iron was conspicuous in cells with a phenotype suggesting oligodendrocytes, with accompanying neuronal pathology and neuronal loss. Neurons still survived, however, despite extensive adjacent glial iron deposition, suggesting neuronal loss is a downstream event. Typical age-related neurodegenerative pathology was not normally present. Uniquely, the extensive aggregates of ubiquitinated ferritin identified indicate that abnormal FTL can aggregate, reflecting the intrinsic ability of FTL to self-assemble. Ferritin aggregates were seen in neuronal and glial nuclei showing parallels with Huntington's disease. There was neither evidence of oxidative stress activation nor any significant mitochondrial pathology in the affected basal ganglia. **Conclusions**: HF shows hallmarks of a protein aggregation disorder, in addition to iron accumulation. Degeneration in HF is not accompanied by

Correspondence: Dr Marzena Kurzawa-Akanbi, Biosciences Institute, Newcastle University, International Centre for Life, Central Parkway, Newcastle upon Tyne NE1 3BZ, UK. Tel: +44 (0)191 241 8818; Fax: 0191 241 8666; E-mail: marzena.kurzawa2@ncl.ac.uk

age-related neurodegenerative pathology and the lack of evidence of oxidative stress and mitochondrial damage suggests that these are not key mediators of neurodegeneration in HF, casting light on other neurodegenerative diseases characterized by iron deposition.

Introduction

Abnormal metabolism of iron has been observed extensively in common neurodegenerative disorders such as Alzheimer's disease (AD) and Parkinson's disease (PD) [1–3], although it remains unclear if this is a secondary effect of neurodegeneration, or whether it directly contributes to cell death. For example in PD, the substantia nigra has been shown to be particularly vulnerable to iron-mediated damage of dopaminergic neurons [4–6] possibly due to the development of reactive oxygen species (ROS) [7], whereas in AD subtle differences in the localization of iron in relation to neurons and the uptake of iron by microglia and astrocytes following cell death suggest that iron accumulation may be a secondary phenomenon of cellular injury [3,8] (for review see [9]).

Neuroferritinopathy (NF) or hereditary ferritinopathy (HF) is one of several Neurodegeneration with Brain Iron Accumulation (NBIA) disorders and occurs commonly due to a frameshift mutation in the light-chain of ferritin (FTL), resulting in an elongated C-terminus to the ferritin monomer and an altered amino acid sequence [10–12]. This change in the ferritin monomer may result in an increased propensity of iron to leak from ferritin oligomers, and associates with iron accumulation within the brain [10,13,14].

Unlike other NBIA disorders, HF is a late-onset autosomal dominant disorder, and one of the only disorders in which the primary metabolic defect is within an iron metabolism protein, rather than a consequence of metabolic dysfunction which is not directly associated with iron metabolism [15,16]. In addition, the spatial deposition of iron in neuroferritinopathy appears similar to the iron deposition seen in the normal ageing brain [2,17]. Therefore, HF could be considered to exhibit the closest model of 'exaggerated' iron accumulation found in normal ageing, and thus the best *in vivo* opportunity to understand the mechanism by which iron deposition may contribute to neuronal death and neuropathology seen in other NBIA disorders.

Here we confirm that in HF; (i) iron deposition follows the normal regional accumulation of iron in the ageing brain, (ii) occurs diffusely throughout the brain, particularly in glia, but also neurons, (iii) does not cause significant ROS production or mitochondrial DNA mutations, (iv) polyubiquitination of ferritin occurs, and (v) that intracellular and intranuclear aggregates of FTL develop in a manner analogous to CAG repeat disorders.

Materials and methods

Post mortem brain histology and iron histochemistry

Fixed and frozen *post mortem* brain tissue from six individuals were utilized within this study. All procedures were approved by the National Health Service Local Research Ethics Committee and appropriate informed consent was obtained from donors or next of kin for tissue donation. Neuropathology of paraffin-embedded tissue sections (10 μm) used routine haematoxylin and eosin and luxol fast blue/cresyl fast violet to demonstrate myelin and neurons. Iron histochemistry used the DAB intensification procedure applied to Perls' or Turnbull's Prussian Blue reaction [2,18,19] and was used to demonstrate ferric (Fe^{3+}) or endogenous ferrous (Fe^{2+}) forms of iron deposition (Supplementary Methods).

Immunohistochemistry

Tissue sections were stained with antibodies to GFAP, ferritin, amyloid-beta (4G8), CD68, HLA-DR/DP/DQ, a phosphorylated epitope of tau (AT8), heavy neurofilament, ubiquitin or alpha-synuclein (KM51) (Supplementary Methods).

Haem oxygenase-1 (HO-1) immunohistochemical detection was performed on 10 μm paraffin sections of the following brain areas: frontal cortex, motor cortex, cerebellum including dentate nucleus, brainstem, anterior basal ganglia, basal ganglia at the globus pallidus, thalamus, hippocampal CA1 and CA2 regions, dentate

gyrus, entorhinal cortex and substantia nigra (Supplementary Methods).

Brain protein homogenate preparation, fractionation and western blot

Frozen-unfixed tissue blocks of the frontal cortex or lateral cerebellum were available from four cases with HF (Cases II, III, IV and VI). Tissue was homogenized in an extraction buffer consisting of 0.2 M triethylammonium bicarbonate (pH8.0, TEAB, Sigma) and protease inhibitor cocktail (Roche), following which samples were prepared for western blotting or fractionated into detergent soluble and insoluble fractions (Supplementary Methods).

Native page

Digitonin or Triton X-100 soluble tissue fractions were subjected to native PAGE analysis using the Native PAGE Novex Bis-Tris system (Life Technologies) components. Following electrophoresis, western blot was performed with several modifications to the standard protocol (details in Supplementary Methods).

Detection of protein carbonyls and Cathepsin D/E activity

Oxidative modifications in proteins were detected using the OxyBlot protein oxidation detection kit (Millipore). Cathepsin D and E activities in frontal cortex samples were measured using a kinetic assay described previously [20] (Supplementary Methods).

Inductively Coupled Plasma Emission Mass Spectrometry (ICPMS)

Metal levels were determined in frozen tissues from cases II, III and IV using ICPMS utilizing a standard additions approach with multielement standards. Tissue samples were wet digested with nitric acid and analysed using a Thermo X Series 2 mass spectrometer (Supplementary Methods).

Mitochondrial DNA (mtDNA) single-nucleotide variant analysis

Frozen unfixed *post mortem* tissue blocks containing the frontal cortex, motor cortex, cerebellum, globus pallidus, putamen and thalamus were dissected and DNA was extracted (Supplementary Methods). DNA was analysed for heteroplasmic and homoplasmic mtDNA point mutations using high-depth amplicon-based sequencing [21]. The data were analysed using an in-house developed bioinformatic pipeline [21]. The minimal coverage at a minimal read depth $1500 \times$ was 96.6% (average 99.2%). The minimal variant frequency was considered to be 1%.

Statistical analysis

Statistical analysis was performed in IBM SPSS 22 and GraphPad Prism 8. Graphs were generated in Microsoft Excel 2010 or GraphPad Prism version 5.04. Data were analysed for normality using Shapiro–Wilk test. Statistical significance was determined based on parametric (independent samples test) or nonparametric (Mann–Whitney test) methods and a significant difference was considered when $P \leq 0.05$.

Results

Clinical presentation of HF cases

All patients of this extended pedigree carried the previously reported *460InsA* mutation in exon 4 of *FTL* that elongates the C-terminal region of the FTL protein [10]. Patients showed symptoms typical of the detailed clinical descriptions of HF presentation and progression provided previously [22]. Gender of individuals has been masked where possible for the purposes of maintaining anonymity for families in a rare disorder.

Case I: A 51-year-old individual and a carrier of the *460InsA* mutation due to detection in a first-degree relative. The patient died from unrelated causes prior to the onset of major neurological symptoms.

Case II: A 53-year-old patient who presented to neurology following the diagnosis of HF in first-degree relative. A CT scan at presentation showed no abnormality within the basal ganglia, and the patient was asymptomatic at initial review. Five years later (aged 58), the patient showed a symmetrical, but mild dyskinesia of the upper limbs, together with an orofacial dyskinesia characterized by pursing of the lips. On examination the patient also exhibited occasional choreiform movements of the upper limbs, were mildly ataxic, and had a cerebellar dysarthria. Informal testing of memory and intellect

was deemed to be normal, although affect was slightly disinhibited. At age 62, an MRI brain scan showed increased T2 signal in the basal ganglia along with mild generalized cerebral and cerebellar atrophy. Over the next 3 years neurological symptoms progressed, with a deterioration of hyperkinetic upper limb movements and progressive memory impairment. At age 65, a repeat MRI and CT examination again showed bilateral abnormalities in the basal ganglia indicating increased iron signal and now cavitation. At age 69, the patient was immobile, fully dependent for all activities of daily living and aphasic. Death was due to aspiration pneumonia 11 years after the onset of symptoms.

Case III: A 58-year-old patient who presented with a 5-year history of involuntary movements of the left foot, together with a 2-year history of involuntary movements of the left upper limb. Over the next 6 months, the patient also developed a progressive dysphagia for solids and liquids and progressive dysphonia. Neurological examination revealed an orofacial dyskinesia, and choreiform movements of the left arm only. One parent had been given a clinical diagnosis of Huntington's disease, though never received a molecular diagnosis. A CT scan of the brain showed bilateral cavitation within the basal ganglia with a normal caudate nucleus. An MRI scan showed changes associated with iron deposition within the basal ganglia. The patient died 3 years after presentation.

Case IV: A 41-year-old patient presented with a 4-year history of a mild spastic paraparesis. Five years later these pyramidal symptoms had also developed symmetrically in the upper limbs, and lower limb pyramidal features had also advanced, although the plantars remained downgoing. In addition, dystonic movements had also developed in the left upper limb. At age 46, neuropsychiatric testing showed reduced verbal memory and processing speed with dysarthric speech consistent with a cerebellar dysarthria. CT imaging of the brain showed discrete lesions in both putamen with MRI imaging showing high T2 signal in the putamen and globus pallidus consistent with iron deposition. At age 47, pyramidal tract features, cerebellar ataxia and memory were noted to have deteriorated further. At age 50, the dystonic gait was particularly troublesome, and symptoms slowly deteriorated until the patient died at the age of 55.

Case V: A 47-year-old patient who presented with a slowly progressive left-sided hemiparesis. There was gradual deterioration over the subsequent 10 years, with progressive weakness and spasticity predominantly affecting the left side. Speech gradually deteriorated from mid-50s, and at 61yrs, dysphagia and dysphonia were prominent. At age 61, the patient had also developed a mild deficit in short-term memory on formal cognitive testing, together with both lower and upper limb dystonia. There was no ataxia. An MRI scan was done at age 61 which showed cystic cavitation of the putamen and globus pallidus bilaterally. There was continued deterioration over the next 5 years with the patient eventually unable to walk, requiring institutional care including enteral feeding. The patient died at the age 66 due to bronchopneumonia.

Case VI: A 50-year-old patient who presented with involuntary choreiform movements of their right hand. Over the next 10 years, the upper limb chorea became bilateral, and by the age of 60 they had also developed significant dysphagia and dysarthria. Aged 62 they had a profound gait disorder, though it remains unclear whether this was due to dystonia or ataxia. At age 75, MRI scan showed bilateral symmetrical lesions through the globus pallidus, putamen, caudate and subthalamic nucleus. At age 75, the patient was wheelchair bound, aphasic, severely dysphagic and a rapid decline in cognition was noted, though this was uncharacterized clinically. The patient died at the age of 76 because of bronchopneumonia. Details of this individual have been reported previously [23].

Liver pathology

Haematoxylin- and eosin-stained sections of *post mortem* liver (cases I, III and VI) showed 5–20 μm diameter roughly spherical eosinophilic inclusions with a pale halo in hepatocytes, typically within nuclei, and diffusely distributed smaller inclusions throughout the cytoplasm as observed previously [10,11]. Staining with Perls' showed the presence of iron within the inclusions and cell nuclei stained for ferritin (Figure 1). Histology of ventricular heart tissue showed low level intranuclear staining for ferritin, although Perls' stain did not show the presence of significant iron. Sections of skin tissue showed diffuse staining with Perls' iron and intranuclear staining of cells within the basal epidermis and within glandular cells with FTL IHC although inclusions were not observed (Figure 1).

Macroscopic CNS pathology

Pathology focussed on the basal ganglia (Figure 2) and was consistent with neuroimaging findings in HF [22,24,25] (see Figure S1) with a gradation of pathology from mild in case I to severe in cases III, V and VI. In all cases, a brown discoloration of the basal ganglia was observed, particularly the remains of the globus pallidus and putamen, but also in the substantia nigra pars reticulata, red nucleus, cerebellar dentate nucleus, and to a lesser extent, the subthalamic nucleus and caudate. Cystic lesions were observed in the internal medullary lamina between the globus pallidus and putamen in case I, which was enlarged in case II, and marked in cases III–VI with cavitation extending throughout the external globus pallidus and within the putamen, with little pallidal or putaminal tissue remaining (Figure 2). In case III, cavitation in the dentate nucleus and substantia nigra was also noted. The cerebellum showed no major atrophy and the brainstem appeared normal. In the cerebral hemispheres there was some cortical deep white matter pallor in case III and VI.

Microscopic pathology

Basal ganglia Microscopic pathology followed macroscopic pathology, being least severe in case I, intermediate in case II and most severe in cases III–VI (Figure S2). On microscopic examination, abundant eosinophilic, roughly spherical inclusions up to 50 μm in diameter were
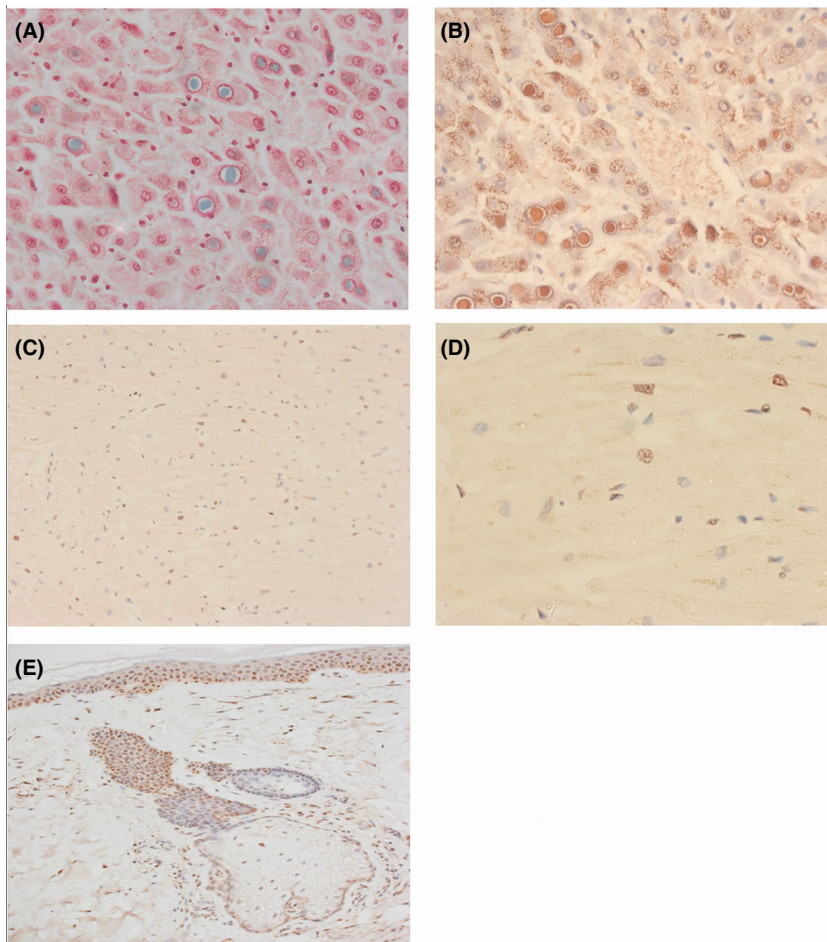

Figure 1. Peripheral pathology in Hereditary Ferritinopathy. Liver tissue shows the presence of widespread intracellular inclusions containing iron (A; Perls' Neutral Red × 40 magnification) and Ferritin L-chain (B; × 40 magnification) typically within cell nuclei. Ventricular myocytes demonstrate intranuclear ferritin staining (C; × 10 magnification, D; × 40 magnification) although iron staining is not apparent (not shown). (E) Skin section showing the presence of intranuclear FTL staining and diffuse staining of dermis (× 20 magnification).
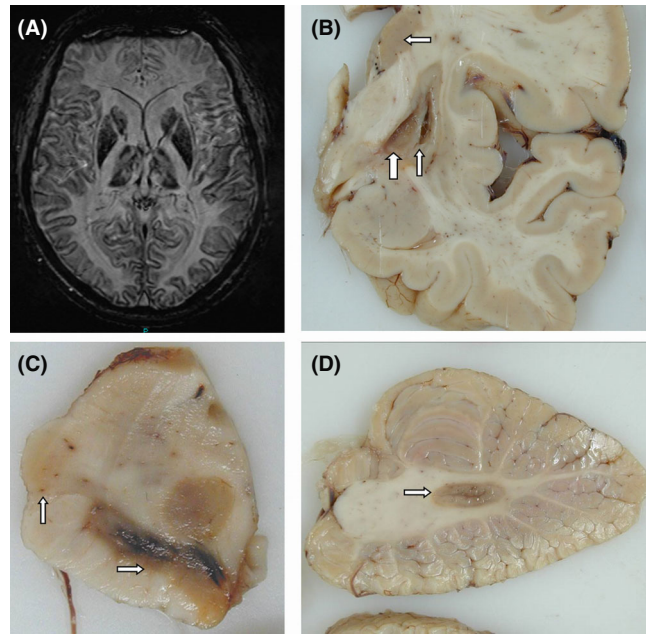
Figure 2. Macroscopic pathology in HF. (**A**) MRI image of an individual with HF in an advanced stage with cavitation of the basal ganglia and decreased signal intensity in thalamus and lower layers of the cerebral cortex. Coronal sections of fixed brain tissue: (**B**) In case III, there are cystic cavities in the globus pallidus (broad vertical arrow) and within the putamen (narrow vertical arrow), with sparing of the caudate nucleus (horizontal arrow). The cerebral cortex shows discoloration in the lower layers at the border with white matter. (**C**) Midbrain from Case III showing normal melanization, but with diffuse brown discoloration of the substantia nigra pars compacta and pars reticulata, along with cerebral peduncles (horizontal arrow). There is some discoloration of the medial geniculate body (vertical arrow). (**D**) Cerebellum from Case III showing the dentate nucleus with brown discoloration and possible cavitation (arrow). The cerebellar cortex appears normal.

observed in the remaining putamen and globus pallidus surrounding the cavity (Figure 3). Histochemistry showed iron predominantly in the Fe^{3+} state (Perls' stain; Figure **3A**), and lower levels of Fe^{2+} (Turnbull's stain). Inclusions were positive for ferritin although some of the largest were unstained (Figure **3B**), with ferritin staining also present in neuronal and some glial nuclei. Iron-positive inclusions were variably positive for ubiquitin (Figure **3C**), and either free in the neuropil or cell associated and involved cells with the morphology of microglia, astrocytes or oligodendrocytes (Figure 3E,F). Many inclusions showed immunocytochemical profiles which may suggest a neuronal origin (e.g. neurofilament (Figure **3H**), and ubiquitin) and were argyrophilic (Gallyas silver).

Iron staining showed a rim of iron-rich glial cells and inclusions surrounding the basal ganglia that was prominent in most cases (e.g. Figure S2), a feature seen in MRI imaging [24]. Adjacent to the cystic lesions, reactive GFAP-positive astrogliosis and reactive HLA-DR/DP/DQ immunopositive microglia-like cells were present (Figure S3). Cells with a morphology similar to

oligodendrocytes in the remaining laminae of the globus pallidus and putamen showed iron- and ferritin-positive intracytoplasmic inclusions (Figure S4). Small-rounded cells, often appearing as a linear arrangement of cells, and with the appearance of oligodendrocytes, were observed in deep white matter tracts and showed extensive intracytoplasmic iron, accompanied by ubiquitin-positive axonal profiles and spheroids.

Neuronal loss was evident in the globus pallidus in III–VI, but not evident in case I despite iron deposition (Figure 4A,B) and gliosis, and mild in case II, with in cases IV–VI very few pallidal neurons remaining due to cavitation. Large neurons in the putamen were readily evident in case I (Figure **4G**), diminished in case II and virtually absent in cases III–VI. In all cases, some small putaminal neurons were still apparent near the cavity. Nuclear neuronal ferritin or iron staining and a background cytoplasmic staining with granular cytoplasmic iron-positive profiles were observed in the remaining globus pallidus (Figure 4A–E). Neurons were observed surrounded by iron reactive inclusions suggesting accumulation of iron and ferritin in degenerated satellite
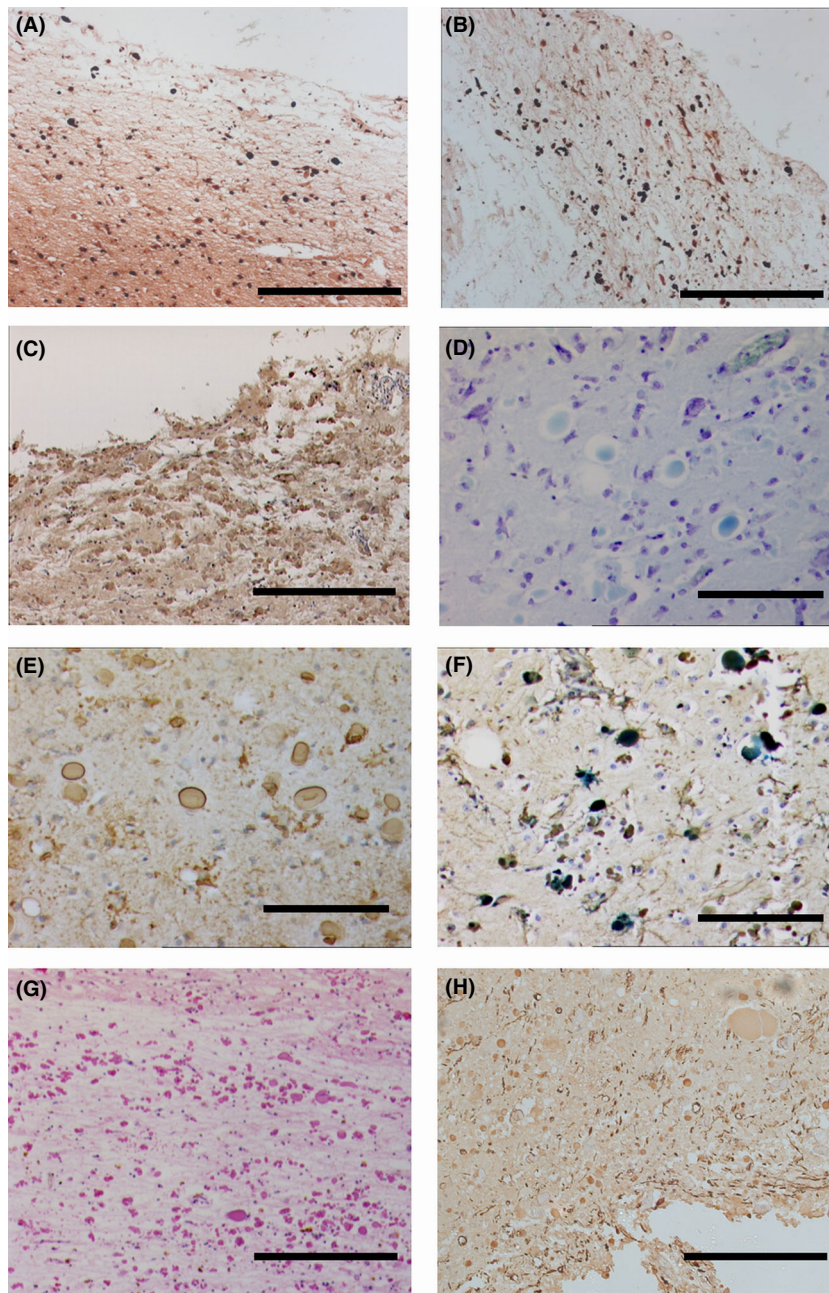
Figure 3. Microscopic pathology of basal ganglia in HF. (**A**) Border of the globus pallidus cyst showing granular iron/ferritin bodies stained heavily for iron (Perls' method with DAB intensification; Case VI). (**B**) Ferritin content of the iron/ferritin bodies (FTL IHC) which are (**C**) only weakly reactive to ubiquitin (IHC for ubiquitin). (**D**) Section through the anterior globus pallidus showing surviving large neurons at an early disease stage (CFV; case I). (**E**) Case I showing roughly spherical iron ferritin bodies of varying size in the cytoplasm and in cellular processes of cells with the morphology of microglia and oligodendrocytes, and also free in the neuropil (FTL IHC). (**F**) Iron content within glial cells, showing the presence of iron within glial processes (Perls' method). (**G**) Abundant eosinophilic profiles, corresponding to the iron/ferritin bodies, in the basal ganglia region that also stain for (**H**) neurofilament along with axonal profiles. (Scale Bars: A, B, C, G, H = 300 μm; D, E, F = 100 μm).

glia (Figure **4F**). In areas of the putamen in case I, large neurons could be observed filled with iron. Many of the larger iron inclusions in the neuropil had a form suggesting a neuronal origin. The neurons of the nucleus basalis of Meynert were preserved in all cases despite iron-positive inclusions throughout the

neuropil. In cases III, V and VI, phospho-Tau (AT8) and scattered alpha-synuclein (KM51) positive neurites were observed in the neuropil (Figure S5).

Midbrain and brainstem   The substantia nigra showed minimal pigmented neuron loss in cases I and II, but extracellular neuromelanin in cases III–VI. In the pars reticulata, nonpigmented neurons were present and showed ferritin and accompanying iron deposition, along with scattered iron- and ferritin-positive inclusions and iron-containing glia with a morphology similar to oligodendrocytes and microglia. Immunostaining for phospho-Tau (AT8) was negative with the exception of case V, which showed scattered neuritic staining. Alpha-synuclein staining demonstrated rare positive neurites in cases II, III, V and VI within the pars compacta and rare Lewy bodies in case VI (Figure S5). The subthalamic nucleus and the red nucleus showed changes similar to those in the globus pallidus and putamen, but in a less advanced state. Only mild changes were present in the thalamus including iron and ferritin inclusions with no evidence of major degenerative changes.

Iron and ferritin deposition were minimal or absent in the pons and medulla and the pyramidal tracts appeared normal. Scattered AT8-positive neurites were seen in the dorsal motor nucleus of the vagal nerve in cases V and VI. Scattered alpha-synuclein-positive neurites in the dorsal motor nucleus, medullary reticular formation and locus coeruleus were seen in cases V and VI.

Cerebellum   The cerebellar dentate nucleus showed neuronal loss in case II, which was extensive in cases III–VI, with surrounding demyelination. There was prominent iron and ferritin deposition both within and as a rim surrounding the nucleus (Figure S6B) predominantly in GFAP-positive astrocyte-like and HLA-DR/DP/DQ or CD68-positive microglia-like cells. Ubiquitinated profiles were also present within the dentate nucleus. Oligodendrocyte-like cells and to a lesser extent cells with a morphology similar to microglia were observed in various stages of iron and ferritin loading from small dust like intracytoplasmic inclusions, to large accumulations that almost obliterated the cell. Similar changes were seen in white matter cells with features suggestive of oligodendrocytes (Figure S6C). Changes in the cerebellar cortex were mild and consisted of iron-positive cells with a Bergmann glia-like phenotype

(Figure S6E, F) and intranuclear Purkinje cell ferritin and iron staining (Figure S6D) with mild Purkinje cell loss in cases III–VI.

Cerebral cortex and white matter   Within the cerebral cortex, iron- and ferritin-positive microglia-like and oligodendrocyte-like cellular profiles were present throughout the cortical grey, particularly in a perineuronal location, these being notable in the hippocampal subiculum (Figure S7E). Iron- and ferritin-positive oligodendrocyte-like cells occurred throughout the white matter. Major neuronal loss in neocortical or archicortical grey matter, including the hippocampus was not evident (Figure S7). Cases V and VI showed AT8-positive phospho-Tau positive neurites in the hippocampus, entorhinal cortex and amygdala (Braak stage II/III; Figure S5E,F). The superficial and deep white matter tracts showed ubiquitin-positive axonal profiles particularly in cases III, V and VI.

Metal levels in HF

We determined levels of several metals in cases (II, III and VI) of HF where frozen tissue was available using ICPMS (Table 1). Levels of iron in the globus pallidus tissue were slightly, but not significantly elevated. In the putamen, iron levels were slightly reduced compared to controls. Iron levels were significantly increased in frontal cortex, motor cortex and thalamus in HF compared to controls, but not in cerebellum. In general copper levels were reduced in several regions in HF, and this was significant in the putamen, motor cortex and thalamus. Manganese and zinc levels were generally unchanged or only slightly reduced in HF.

Ferritin alterations in HF

In the frontal cortex, we observed a trend towards an increase in FTL levels ($P = 0.08$), a significant increase in total ferritin levels ($P < 0.01$) and a significantly altered FTH/FTL ratio in HF ($P < 0.01$; Figure 5). Analysis of native ferritin complex in controls revealed the presence of one band of 480 kDa, corresponding to the 24-mer ferritin complex in control frontal cortex (Figure 5). In HF frontal cortex and cerebellum, however, we detected ferritin oligomers of approximate molecular weight 720 and 1000 kDa, that were immunopositive for FTL and FTH. This observation made us explore
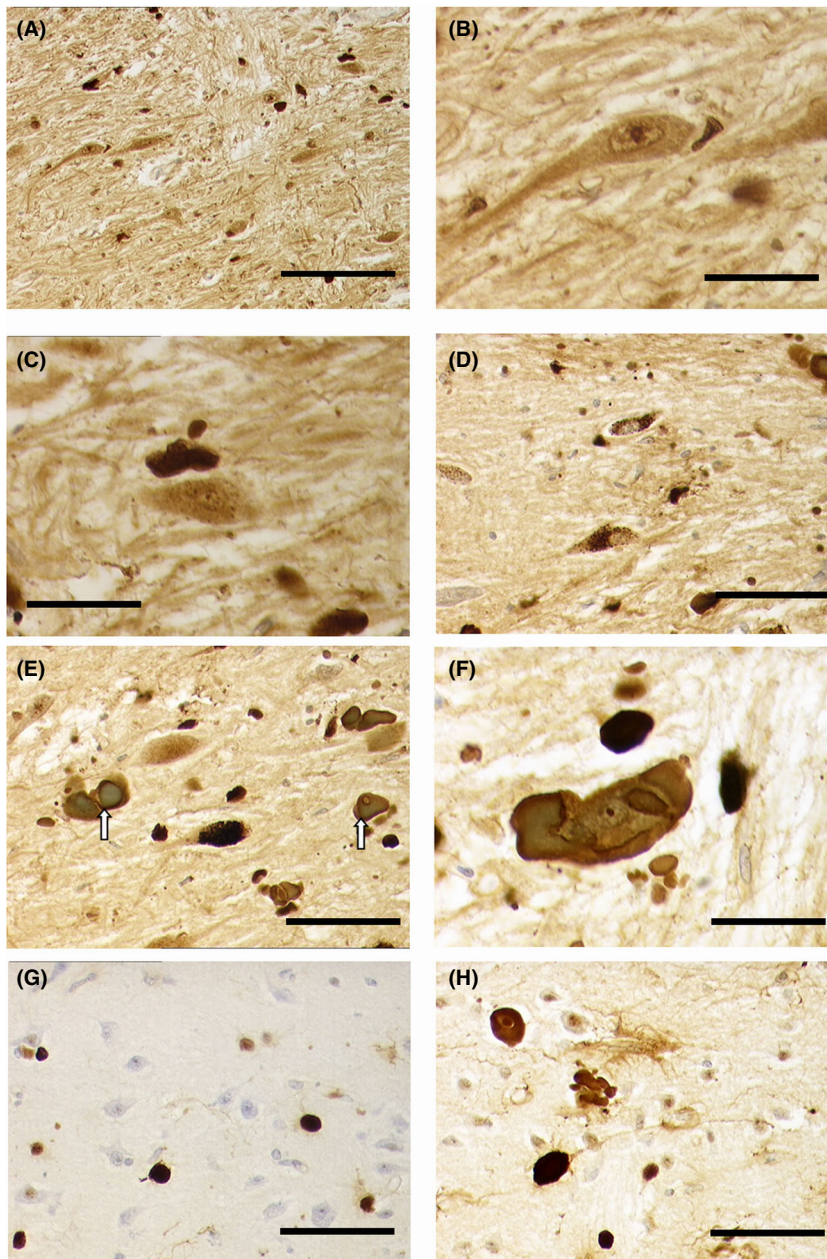
Figure 4. Neuronal iron staining in the basal ganglia. (**A**) Medial globus pallidus from case I showing iron-stained neurons. Neurons show variable iron reactivity: (**B**) diffuse cytoplasmic staining with strong nuclear staining; (**C**) fine granular cytoplasmic staining; (**D**) increased cytoplasmic iron content; (**E**) iron/ferritin bodies possibly derived from degeneration of overloaded neurons (arrows). (**F**) Iron-containing neurons are surrounded by iron/ferritin bodies which may represent remnant satellite glial cells. (**G**) Neurons in the lateral putamen show normal neuronal morphology with absent iron staining despite the presence of iron/ferritin bodies within the neuropil. (**H**) In contrast, the medial putamen adjacent to the cystic cavity shows iron-stained neurons with iron extending out into dendritic processes (Perls' method with DAB intensification). (Scale Bars: A = 100 μm; D, E, G, H = 50 μm; B, C = 25 μm).

further the solubility of ferritin. Frontal cortex and cerebellum samples were fractionated (Figure S8) and analysed by SDS-PAGE. High molecular weight protein species, immunopositive for FTL, were detected in all fractions of HF brain preparations, including 88% and 98% formic acid fractions (Figure 6). These ferritin oligomers in the formic acid fractions represent aggregated forms of ferritin, most likely stabilized by covalent bonds,

Table 1. Metal levels in HF

		Globus pallidus	Putamen	Frontal cortex	Motor cortex	Thalamus	Cerebellum
^{56}Fe	Control	246692 ± 73229	171962 ± 30068	50913 ± 16441	67419 ± 11619	73476 ± 20912	47590 ± 15674
	HF	664228 ± 798814	170011 ± 61764	76647 ± 11158*	113526± 44973*	122186± 23807*	58624 ± 6115
^{55}Mn	Control	592 ± 60	597 ± 56	217 ± 54	240 ± 35	463 ± 104	323 ± 44
	HF	1858 ± 2622	442 ± 46*	243 ± 55	276 ± 74	439 ± 112	351 ± 21
^{63}Cu	Control	7172 ± 771	8151 ± 1724	4019 ± 1503	4717 ± 564	5269 ± 1298	5469 ± 1005
	HF	15465 ± 20550	3520 ± 968*	2875 ± 445	3222 ± 457*	2841 ± 688*	3892 ± 920
^{66}Zn	Control	14440 ± 1491	15914 ± 1532	13020 ± 3899	12997 ± 1369	14497 ± 2065	12875 ± 1286
	HF	35753 ± 48688	11225 ± 96*	12888 ± 1624	12295 ± 1225	13477 ± 2199	14326 ± 850

Snap frozen-unfixed tissue samples were wet digested in nitric acid and metals determined using a standard additions method with inductively coupled plasma emission mass spectrometry (ICPMS). Metal levels are presented as ng metal/mg wet weight of tissue with control samples (Age 68.2 years ± 4.8 years [SD] range 63–74: 2F/4M) and HF cases (Age 61.3 years ± 6.5 years [SD] range 55–64: 3F). Comparisons were made with unpaired Mann–Whitney U-test assuming unequal variances and uncorrected.
*P values < 0.05.

as they were resistant to formic acid and TCEP-HCl. Monomeric FTL and FTH subunits were also present in the control brain formic acid preparations, suggestive of age-related haemosiderin accumulation and that ferritin, given its homopolymeric nature, can aggregate spontaneously. Due to the presence of aggregated protein and the presence of ubiquitin in inclusions we sought to determine if ferritin itself is ubiquitinated and particularly as polyubiquitination via the K48-linkage is known to target proteins for proteasomal degradation and ferritin monomers can undergo proteasomal degradation [26,27]. We immunoprecipitated ferritin from the frontal cortex and cerebellum and probed for polyubiquitination using SDS-PAGE and immunoblotting. We detected two bands of polyubiquitinated FTL, a fainter band migrating at approximately 27 kDa and a major band at approximately 55 kDa potentially representing a dimer, in both HF and controls (Figure 7). These polyubiquitinated bands were readily observed in soluble extracts of total brain protein in HF and to a lesser extent in control tissue (Figure S9). Interestingly, the degree of polyubiquitination in urea soluble tissue extracts in HF seemed to be lower than in controls, in particular in a sample showing the highest levels of detergent resistant ferritin oligomers. This observation may indicate failed clearance of ferritin in HF, possibly due to misfolding and aggregation, which may partially account for the accumulation of ferritin seen in HF.

Iron transport protein levels are not affected in HF

Due to the elevated iron and ferritin in HF, we determined if iron entry into the brain is regulated by determining the expression of iron import proteins, ferroportin 1 and transferrin receptor 1. There were no significant changes in ferroportin 1 or transferrin receptor 1 protein levels (Figure S10).

Altered mitochondrial iron metabolism in HF

As iron within the brain is predominantly used for oxidative metabolism in mitochondria, the handling and use of iron was determined within HF patient brain samples. In HF frontal cortex, levels of mitochondrial proteins were unaltered with levels of the major mitochondrial protein VDAC1/porin, frataxin, NDUFB8, ubiquinol-cytochrome c reductase core protein 1, MTCO2 and
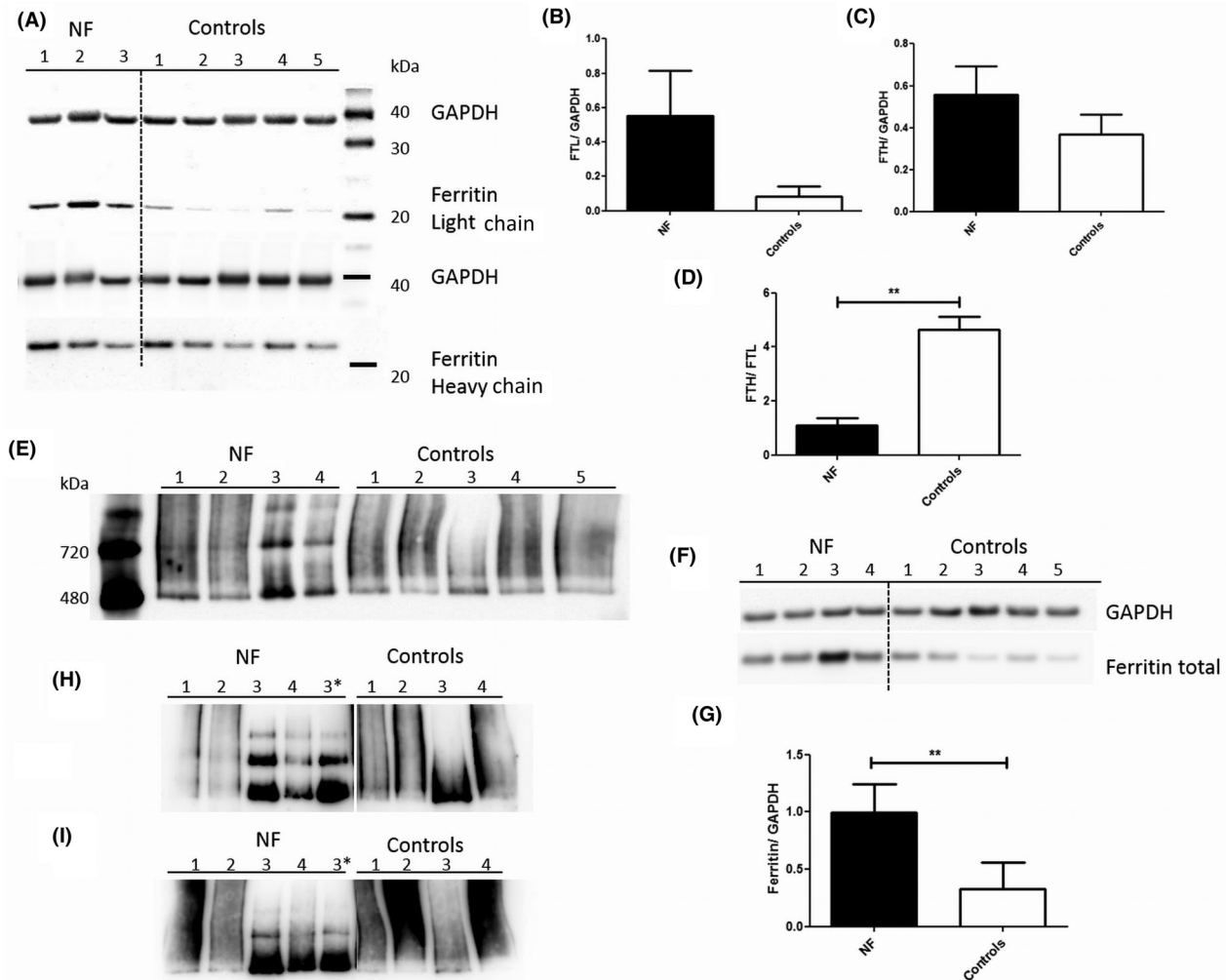
Figure 5. Analysis of ferritin in Hereditary Ferritinopathy/Neuroferritinopathy and controls. Samples of frontal cortex tissue were analysed using western blotting and probed using ferritin-specific antibodies (**A**). Trend towards increased levels of both FTL (**B**) and FTH (**C**) were seen in HF (NF) in comparison to control tissue samples, with an altered FTH/FTL ratio (**, $P < 0.01$, unpaired t-test) (**D**). Native PAGE analysis of the ferritin complex (**E**) to identify the ferritin holoprotein demonstrated the presence of two to three bands migrating at 480 kDa, 720 kDa and approximately 1000 kDa in HF (NF) and only one band showing the ferritin holoprotein monomer in controls when probed with antibodies recognizing both FTL and FTH. For comparison, western blot analysis shows levels of ferritin in the same cases (**F**, **G**). Native PAGE and immunoblotting using antibodies specific to FTL (**H**) and FTH (**I**) confirmed the presence of ferritin oligomers in the patients. 1, 2, etc. – patient and control frontal cortex; 3* - Cerebellum.

ATP5A unchanged (not shown). NDUFS1 was, however, significantly decreased in frontal cortex of HF, by 15% compared to controls ($P = 0.0223$) (Figure S11). Mitochondrial DNA (mtDNA) from HF (frontal cortex, globus pallidus, thalamus, cerebellum, putamen and motor cortex) showed no significant differences in the copy number (Figure S12), or the presence of major deletions in any brain areas compared to controls. Next-generation sequencing also did not reveal a higher mutational burden in the severely affected globus pallidus compared to

the relatively spared cerebellum (Figure S13 and Table S4).

No major evidence of oxidative stress in HF

As iron has been linked to reactive oxygen species generation, we explored oxidative stress markers in HF brains. Immunohistochemical analysis of haem oxygenase 1 in multiple brain regions did not show a statistically significant difference in levels in HF compared to
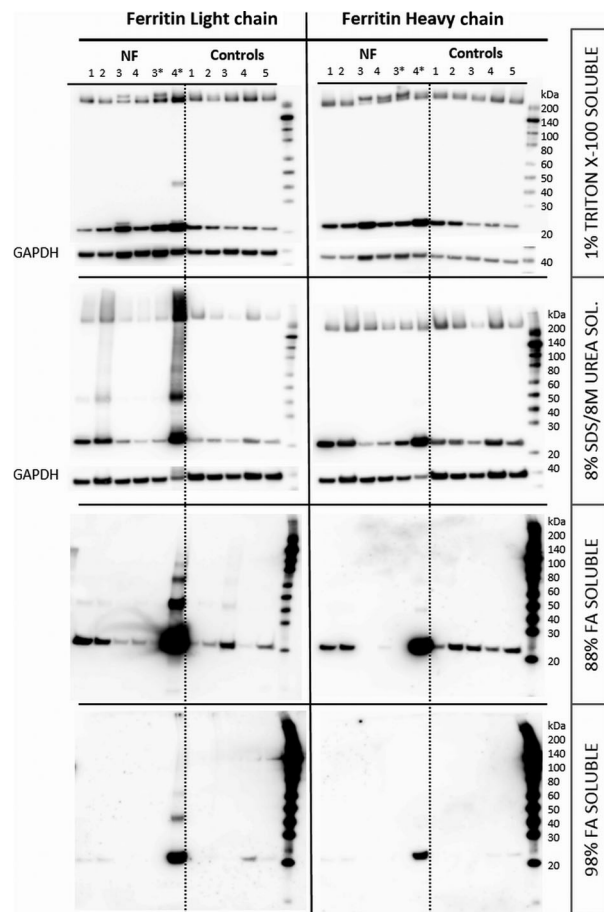
Figure 6. Solubility of ferritin in HF. Tissue samples were sequentially fractionated based on protein solubility properties and analysed by SDS PAGE and immunoblotting using anti-FTL and anti-FTH antibodies. GAPDH was used as a loading control when suitable. Oligomers of FTL are seen in all fractions of HF brain extracts. The presence of higher molecular weight species of FTL in the formic acid purified fractions suggests the formation of covalent bonds between FTL molecules. Age-matched controls were not free from the detergent resistant and formic acid soluble ferritin possibly due to the presence of haemosiderin, however, the formation of oligomers was generally reduced compared to HF.

aged controls (Figure S14 and Table S5). Analysis of protein carbonyl groups, markers of protein oxidative changes, in frontal cortex did not reveal any significant changes in HF (Figure S15). Similarly, we saw only a small elevation in SOD1 expression, but no change in SOD2 or HSP70 (Figure S15).

Lysosomal functions in HF

As ferritin can be degraded by lysosomes [28–32] we explored lysosomal dysfunction as contributing to

accumulation of ferritin and ferritin oligomers. Cathepsin D and E enzyme activities showed no significant change in HF (Figure S16). Lysosomal markers, LAMP1, LAMP2 and TFEB (Transcription Factor EB) also showed no significant differences, however, cathepsin D protein was significantly reduced in HF ($P = 0.003$) (Figure S16).

Discussion

This study significantly advances our understanding of the neuropathology of hereditary ferritinopathy/neuro-ferritinopathy, highlighting unique pathological features of the disorder and suggesting potential novel mechanisms of neurodegeneration.

Intriguingly when measuring tissue iron content, we observed largely similar overall iron levels in HF cases compared to controls within several brain regions including the putamen and globus pallidus (Table 1). While this may be mediated by cavitation, and therefore the loss of cellular iron in these regions to CSF, the observation of generally reduced copper, zinc and manganese particularly within the putamen, and no down-regulation of iron transport mechanisms suggests that accumulation of iron does not necessarily mediate neurodegeneration in the *FTL 460InsA* mutation. Rather, local cell-specific changes potentially due to FTL accumulation (see below) may underlie these effects through loss of cells manifesting as reduced levels of other metals including copper. The mechanism underlying the dysregulation of additional metals, particularly in the putamen, has not been observed in other forms of NBIA. Similar changes in metals have been observed in the heart in Friedreich's ataxia [33], and therefore a comparable process may occur in other degenerative disorders associated with iron. Understanding the relative contribution of iron and other metals to disease pathogenesis may have significant implications for treatment, including the use of chelation agents being currently trialled for other NBIA disorders.

Histopathological assessment of HF cases showed that excess iron staining within cells in HF closely paralleled normal age-associated iron deposition [17], though potentially to pathological excess within individual cells. In HF, areas such as the globus pallidus, substantia nigra pars reticulata and cerebellar dentate show high intracellular iron staining with the predominant accumulation of iron within glial cells, with their morphology and immunophenotype suggestive of oligodendrocytes and
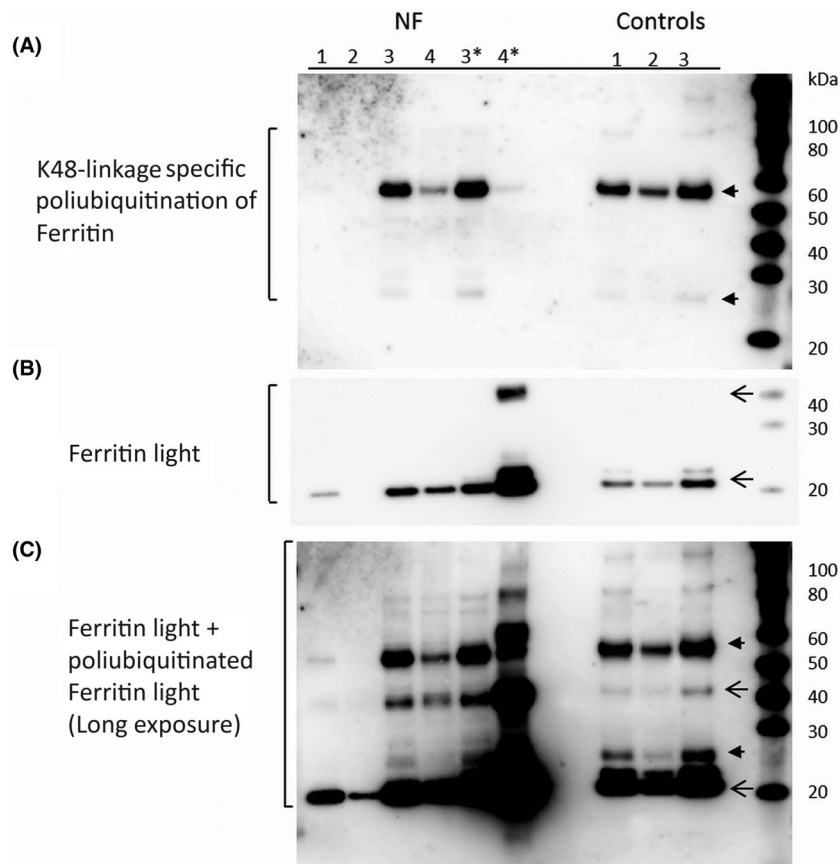
Figure 7. K48-linkage polyubiquitination of ferritin in HF and controls. Immunoprecipitation of ferritin from tissue extracts with western blot analysis indicated K48 polyubiquitination (arrowheads) of ferritin monomer and higher molecular weight (57 kDa) ferritin K48 ubiquitin linkage. Use of FTL antibody showed monomeric ferritin light chain (panel B, ~22 kDa, lower arrow) and in HF potential FTL dimers (~44 kDa, upper arrow). Extended exposure times for blots using both FTL and K48 polyubiquitin antibodies showed K48-ubiquitinated FTL monomers and dimers in both HF and control frontal cortex.

microglia [1,2]. Both cell types in the normal brain are known to contain FTL as the major form of ferritin [1,34] suggesting that the same relative distribution of iron occurs within HF as in the ageing brain at the cellular level, with the deviation from normal levels most likely mediated by altered function of mutant FTL. High-resolution imaging, perhaps using electron microscopy, should, however, be used to definitively determine that nature of these inclusions involves both ferritin and iron, and how these inclusions affect the morphology and potential function of cells. It is of interest that in the case of individuals with the *FTL460InsA* mutation they show dystonia and choreiform movement disorders as the presenting phenotype although cerebellar pathology is readily evident [22,24,25]. In other cases of HF with different mutations, cerebellar features are prominent or the

mutation shows either cerebellar or Parkinsonian features [11,35].

We observed cells with a morphology similar to oligodendrocytes at various stages of iron and ferritin loading, ranging from small cytoplasmic iron and ferritin deposits that gradually appear to coalesce into larger clusters of FTL and iron. Critically, we observed oligodendrocyte-like cell death as a result of this process within key anatomical regions such as the internal medullary laminae between the globus pallidus and putamen, and this is likely to lead to the observed cavitation exhibited as a core feature of HF, in part causing deafferentation. Ongoing cell death in this region and throughout the basal ganglia could result in a self-perpetuating cycle of mutant ferritin production, iron loading and consequent ferritin aggregation, iron release from dead and dying

cells and cellular iron uptake into adjacent cells into an abnormal ferritin. The observed rim of mutant FTL and iron containing GFAP-positive astrocyte like cells and HLA-DR/DP/DQ-positive and CD68-positive microglia-like cells surrounding the basal ganglia and dentate nucleus is consistent with this. It is therefore highly likely to explain the marked cavitation observed in HF which significantly advances our understanding of this ubiquitous feature [36].

While our observations associate neuropathology and cell death with glia in particular regions, we also tested additional possible mechanisms. Previous studies using *in vitro* and *in vivo* models have suggested that neuronal dysfunction may occur because of ROS mediated through acquired mitochondrial dysfunction [37,38]. However, we observed no significant evidence of elevated ROS when testing for oxidative stress markers using a cellular histochemical approach, no evidence of secondary mitochondrial DNA mutations, no major changes in mitochondrial mass, and no differences in almost all OXPHOS proteins to indicate mitochondrial dysfunction. These data provide compelling evidence to suggest that ROS and mitochondrial dysfunction are unlikely to be key mediators of neurodegeneration in HF challenging previous hypotheses [37–39]. They also challenge the idea that oxidative stress due to iron may lead to common neurodegenerative disorders. The HF patients studied here showed little neurodegenerative pathology in the form of NFT or Lewy bodies, although Case II and VI did exhibit very occasional Lewy bodies in the medulla and substantia nigra, and in cases II, V and VI, hyperphosphorylated tau accumulation was present, but at levels similar to normal older persons. Furthermore, while overexpression of mutant FTL leads to oxidative stress in cell and animal models [40,41], similar levels of oxidative stress are not generated in HF. Therefore, modelling HF in cell lines or mice by overexpression, may not reliably recapitulate the cell-type and region-specific vulnerability exhibited in patients.

The observation of ferritin protein and also iron located in the nucleus particularly in neurons but also notably liver hepatocytes, was reminiscent of nuclear protein accumulation seen in CAG repeat disorders such as Huntington's disease and dentatopallidorubroluysian atrophy [42,43]. To the best of our knowledge, protein aggregates have not previously been biochemically observed in HF brain tissue due to the *FTL 460InsA* mutation, although the presence of FTL and FTH monomers and dimers has been shown in putaminal and cerebellar inclusion bodies from a case with the *498-499InsTC* in exon 4 of *FTL* [11]. Certainly, ferritin can localize to the nucleus in some cells and tissues although this is typically FTH and not FTL [44–47]. However, we identified large oligomers of FTL that are resistant to formic acid, appear to be covalently bonded and ubiquitinated. FTL aggregates were not noticeable in controls, and the presence of the FTL mutation in a region of the protein which is important in the folding of the peptide [37,48] suggests that this aggregate is likely to be highly HF specific and may be an exaggerated version of the intrinsic ability of FTL monomers to self-assemble [49]. This aggregation may also lead to some proteasomal inhibition by mutant FTL since excess FTL can accumulate within lysosomes [49] and mutant FTL can reduce proteasomal metabolism [37]. Identification of aggregated ubiquitinated ferritin suggests that the gradual accumulation of iron in the nucleus may be secondary to the nuclear aggregation of FTL, which is impaired in its ability to accumulate iron [37]. In addition, the lack of association between axonal iron deposition and axonal ubiquitination was also striking. This may suggest that iron deposition may not primarily drive neuronal dysfunction in some brain regions, and instead may be driven by ferritin aggregation, supportive of the previously proposed model of ferritin aggregation and toxic gain of function [50], and similar to other neuronal aggregates such as Lewy bodies in PD or Tau in FTD [51], though further work is required to prove this association.

Finally, the finding of widespread neuronal dystrophy and lack of association between neuronal ubiquitination and iron, irrespective of aetiology, also conclusively suggests that HF is not simply a focal iron accumulation disorder involving the CNS, particularly given hepatic pathology observed herein and peripheral organ ferritin inclusion bodies reported elsewhere [11]. HF should be described therefore as a diffuse neurodegenerative disorder despite the ostensibly focal changes observed on radiological imaging and macroscopic neuropathological examination. Such diffuse findings may also help to explain some of the cognitive features observed in the disorder that cannot be entirely explained by focal pathology [24,52].

In summary, we find that the predominant clinical phenotypic features of HF are likely to arise from loss of integrity of the internal medullary lamina of the

globus pallidus, leading to destruction of the basal ganglia. This pathology follows an exaggerated form of the normal age-associated accumulation of iron and ferritin in the brain. The underlying mechanism in HF may not, however, be due solely to iron-mediated oxidative stress, but aggregation of mutant FTL, ubiquitination and inhibition of proteostasis leading to cell death in common with several other neurodegenerative disorders.

Acknowledgements

Ethical approval

All procedures were approved by the National Health Service Local Research Ethics Committee and appropriate informed consent was obtained from donors or next of kin for tissue donation.

Authors' Contributions

MKA, MK, JB, PFC and CMM initiated the research ideas and experimental design. MKA, MK, ET, LR, MJ, SK, LWSAO, AMN, PS, AK, AP, GH, PGI, JA, JB and CMM performed data acquisition, analysis and interpretation. MKA, MK and CMM undertook manuscript drafting and writing. MKA, MK, ET, LR, MJ, SK, LWSAO, AMN, PS, AK, AP, GH, PGI, JA, JB, PFC and CMM carried out critical revision of the manuscript.

Funding information

Competing Interests

The authors report no competing interests.

Data availability statement

The data that supports the findings of this study are available in the supplementary material of this article. Additional data are available from the corresponding author upon reasonable request.

References

1 Connor JR, Menzies SL, St Martin SM, Mufson EJ. Cellular distribution of transferrin, ferritin, and iron in normal and aged human brains. *J Neurosci Res.* 1990; **27**(4): 595–611

2 Morris CM, Candy JM, Oakley AE, Bloxham CA, Edwardson JA. Histochemical distribution of non-haem iron in the human brain. *Acta Anat (Basel).* 1992; **144**(3): 235–57

3 Neumann MA. Langdon Down syndrome and Alzheimer's disease. *J Neuropathol Exp Neurol.* 1967; **26**(1): 149–50

4 Dexter DT, Carayon A, Vidailhet M, Ruberg M, Agid F, Agid Y et al Decreased ferritin levels in brain in Parkinson's disease. *J Neurochem.* 1990; **55**(1): 16–20

5 Gerlach M, Double KL, Ben-Shachar D, Zecca L, Youdim MB, Riederer P. Neuromelanin and its interaction with iron as a potential risk factor for dopaminergic neurodegeneration underlying Parkinson's disease. *Neurotox Res.* 2003; **5**(1–2): 35–44

6 Morris CM, Edwardson JA. Iron histochemistry of the substantia nigra in Parkinson's disease. *Neurodegeneration.* 1994; **3**(4): 277–82

7 Wypijewska A, Galazka-Friedman J, Bauminger ER, Wszolek ZK, Schweitzer KJ, Dickson DW et al Iron and reactive oxygen species activity in parkinsonian substantia nigra. *Parkinsonism Relat Disord.* 2010; **16**(5): 329–33

8 Morris CM, Kerwin JM, Edwardson JA. Non-haem iron histochemistry of the normal and Alzheimer's disease hippocampus. *Neurodegeneration.* 1994; **3**(4): 267–75

9 Belaidi AA, Bush AI. Iron neurochemistry in Alzheimer's disease and Parkinson's disease: targets for therapeutics. *J Neurochem.* 2016; **139**(Suppl 1): 179–97

10 Curtis AR, Fey C, Morris CM, Bindoff LA, Ince PG, Chinnery PF et al Mutation in the gene encoding ferritin light polypeptide causes dominant adult-onset basal ganglia disease. *Nat Genet.* 2001; **28**(4): 350–4

11 Vidal R, Ghetti B, Takao M, Brefel-Courbon C, Uro-Coste E, Glazier BS et al Intracellular ferritin accumulation in neural and extraneural tissue characterizes a neurodegenerative disease associated with a mutation in the ferritin light polypeptide gene. *J Neuropathol Exp Neurol.* 2004; **63**(4): 363–80

12 Nishida K, Garringer HJ, Futamura N, Funakawa I, Jinnai K, Vidal R et al A novel ferritin light chain mutation in neuroferritinopathy with an atypical presentation. *J Neurol Sci.* 2014; **342**(1–2): 173–7

13 Luscieti S, Santambrogio P, Langlois d'Estaintot B, Granier T, Cozzi A, Poli M et al Mutant ferritin L-chains that cause neurodegeneration act in a dominant-negative manner to reduce ferritin iron incorporation. *J Biol Chem.* 2010; **285**(16): 11948–57

14 Muhoberac BB, Baraibar MA, Vidal R. Iron loading-induced aggregation and reduction of iron incorporation in heteropolymeric ferritin containing a mutant light chain that causes neurodegeneration. *Biochim Biophys Acta.* 2011; **1812**(4): 544–8

15 Keogh MJ, Morris CM, Chinnery PF. Neuroferritinopathy. *Int Rev Neurobiol.* 2013; **110**: 91–123

16 Hayflick SJ, Kurian MA, Hogarth P. Neurodegeneration with brain iron accumulation. *Handb Clin Neurol.* 2018; **147**: 293–305

17 Hallgren B, Sourander P. The effect of age on the non-haemin iron in the human brain. *J Neurochem.* 1958; **3**(1): 41–51

18 Hill JM, Switzer 3rd RC. The regional distribution and cellular localization of iron in the rat brain. *Neuroscience* 1984; **11**(3): 595–603

19 Nguyen-Legros J, Bizot J, Bolesse M, Pulicani JP. "Diaminobenzidine black" as a new histochemical demonstration of exogenous iron (author's transl). *Histochemistry* 1980; **66**(3): 239–44

20 Kurzawa-Akanbi M, Hanson PS, Blain PG, Lett DJ, McKeith IG, Chinnery PF et al Glucocerebrosidase mutations alter the endoplasmic reticulum and lysosomes in Lewy body disease. *J Neurochem* 2012; **123**(2): 298–309

21 Pyle A, Hudson G, Wilson IJ, Coxhead J, Smertenko T, Herbert M et al Extreme-depth re-sequencing of mitochondrial DNA finds no evidence of paternal transmission in humans. *PLoS Genet.* 2015; **11**(5): e1005040

22 Chinnery PF, Crompton DE, Birchall D, Jackson MJ, Coulthard A, Lombes A et al Clinical features and natural history of neuroferritinopathy caused by the FTL1 460InsA mutation. *Brain* 2007; **130**(Pt 1): 110–9

23 Ondo WG, Adam OR, Jankovic J, Chinnery PF. Dramatic response of facial stereotype/tic to tetrabenazine in the first reported cases of neuroferritinopathy in the United States. *Mov Disord.* 2010; **25**(14): 2470–2

24 Keogh MJ, Aribisala BS, He J, Tulip E, Butteriss D, Morris C et al Voxel-based analysis in neuroferritinopathy expands the phenotype and determines radiological correlates of disease severity. *J Neurol.* 2015; **262**(10): 2232–40

25 Keogh MJ, Jonas P, Coulthard A, Chinnery PF, Burn J. Neuroferritinopathy: a new inborn error of iron metabolism. *Neurogenetics.* 2012; **13**(1): 93–6

26 De Domenico I, Vaughn MB, Li L, Bagley D, Musci G, Ward DM et al Ferroportin-mediated mobilization of ferritin iron precedes ferritin degradation by the proteasome. *EMBO J.* 2006; **25**(22): 5396–404

27 Rudeck M, Volk T, Sitte N, Grune T. Ferritin oxidation in vitro: implication of iron release and degradation by the 20S proteasome. *IUBMB Life* 2000; **49**(5): 451–6

28 Asano T, Komatsu M, Yamaguchi-Iwai Y, Ishikawa F, Mizushima N, Iwai K. Distinct mechanisms of ferritin delivery to lysosomes in iron-depleted and iron-replete cells. *Mol Cell Biol.* 2011; **31**(10): 2040–52

29 Yang ND, Tan SH, Ng S, Shi Y, Zhou J, Tan KS et al Artesunate induces cell death in human cancer cells via enhancing lysosomal function and lysosomal degradation of ferritin. *J Biol Chem.* 2014; **289**(48): 33425–41

30 Goralska M, Nagar S, Fleisher LN, McGahan MC. Differential degradation of ferritin H- and L-chains: accumulation of L-chain-rich ferritin in lens epithelial cells. *Invest Ophthalmol Vis Sci.* 2005; **46**(10): 3521–9

31 Kidane TZ, Sauble E, Linder MC. Release of iron from ferritin requires lysosomal activity. *Am J Physiol Cell Physiol.* 2006; **291**(3): C445–55

32 La A, Nguyen T, Tran K, Sauble E, Tu D, Gonzalez A et al Mobilization of iron from ferritin: new steps and details. *Metallomics.* 2018; **10**(1): 154–68

33 Kruger PC, Yang KX, Parsons PJ, Becker AB, Feustel PJ, Koeppen AH. Abundance and significance of iron, zinc, copper, and calcium in the hearts of patients with friedreich ataxia. *Am J Cardiol.* 2016; **118**(1): 127–31

34 Kaneko Y, Kitamoto T, Tateishi J, Yamaguchi K. Ferritin immunohistochemistry as a marker for microglia. *Acta Neuropathol.* 1989; **79**(2): 129–36

35 Ory-Magne F, Brefel-Courbon C, Payoux P, Debruxelles S, Sibon I, Goizet C et al Clinical phenotype and neuroimaging findings in a French family with hereditary ferritinopathy (FTL498-499InsTC). *Mov Disord.* 2009; **24**(11): 1676–83

36 McNeill A, Gorman G, Khan A, Horvath R, Blamire AM, Chinnery PF. Progressive brain iron

accumulation in neuroferritinopathy measured by the thalamic T2* relaxation rate. *AJNR Am J Neuroradiol.* 2012; **33**(9): 1810–3

37 Cozzi A, Rovelli E, Frizzale G, Campanella A, Amendola M, Arosio P et al Oxidative stress and cell death in cells expressing L-ferritin variants causing neuroferritinopathy. *Neurobiol Dis.* 2010; **37**(1): 77–85

38 Maccarinelli F, Pagani A, Cozzi A, Codazzi F, Di Giacomo G, Capoccia S et al A novel neuroferritinopathy mouse model (FTL 498InsTC) shows progressive brain iron dysregulation, morphological signs of early neurodegeneration and motor coordination deficits. *Neurobiol Dis.* 2015; **81**: 119–33

39 Vidal R, Miravalle L, Gao X, Barbeito AG, Baraibar MA, Hekmatyar SK et al Expression of a mutant form of the ferritin light chain gene induces neurodegeneration and iron overload in transgenic mice. *J Neurosci.* 2008; **28**(1): 60–7

40 Baraibar MA, Barbeito AG, Muhoberac BB, Vidal R. A mutant light-chain ferritin that causes neurodegeneration has enhanced propensity toward oxidative damage. *Free Radic Biol Med* 2012; **52**(9): 1692–7

41 Barbeito AG, Garringer HJ, Baraibar MA, Gao X, Arredondo M, Nunez MT et al Abnormal iron metabolism and oxidative stress in mice expressing a mutant form of the ferritin light polypeptide gene. *J Neurochem.* 2009; **109**(4): 1067–78

42 Becher MW, Rubinsztein DC, Leggo J, Wagster MV, Stine OC, Ranen NG et al Dentatorubral and pallidoluysian atrophy (DRPLA). Clinical and neuropathological findings in genetically confirmed North American and European pedigrees. *Mov Disord.* 1997; **12**(4): 519–30

43 Ross CA. Polyglutamine pathogenesis: emergence of unifying mechanisms for Huntington's disease and related disorders. *Neuron* 2002; **35**(5): 819–22

44 Linsenmayer TF, Cai CX, Millholland JM, Beazley KE, Fitch JM. Nuclear ferritin in corneal epithelial cells: tissue-specific nuclear transport and protection from UV-damage. *Prog Retin Eye Res.* 2005; **24**(2): 139–59

45 Surguladze N, Patton S, Cozzi A, Fried MG, Connor JR. Characterization of nuclear ferritin and mechanism of translocation. *Biochem J.* 2005; **388**(Pt 3): 731–40

46 Cai CX, Linsenmayer TF. Nuclear translocation of ferritin in corneal epithelial cells. *J Cell Sci.* 2001; **114**(Pt 12): 2327–34

47 Wu T, Li Y, Liu B, Zhang S, Wu L, Zhu X et al Expression of Ferritin Light Chain (FTL) is elevated in glioblastoma, and FTL silencing inhibits glioblastoma cell proliferation via the GADD45/JNK pathway. *PLoS One* 2016; **11**(2): e0149361

48 Harrison PM, Arosio P. The ferritins: molecular properties, iron storage function and cellular regulation. *Biochim Biophys Acta.* 1996; **1275**(3): 161–203

49 Harned J, Ferrell J, Lall MM, Fleisher LN, Nagar S, Goralska M et al Altered ferritin subunit composition: change in iron metabolism in lens epithelial cells and downstream effects on glutathione levels and VEGF secretion. *Invest Ophthalmol Vis Sci.* 2010; **51**(9): 4437–46

50 Baraibar MA, Barbeito AG, Muhoberac BB, Vidal R. Iron-mediated aggregation and a localized structural change characterize ferritin from a mutant light chain polypeptide that causes neurodegeneration. *J Biol Chem.* 2008; **283**(46): 31679–89

51 Spires-Jones TL, Attems J, Thal DR. Interactions of pathological proteins in neurodegenerative diseases. *Acta Neuropathol.* 2017; **134**(2): 187–205

52 Keogh MJ, Singh B, Chinnery PF. Early neuropsychiatry features in neuroferritinopathy. *Mov Disord.* 2013; **28**(9): 1310–3

Supporting information

Additional Supporting Information may be found in the online version of this article at the publisher's web-site:

Data S1. Supplementary methods and figures.